

Article

Ofloxacin Degradation over Nanosized Fe₃O₄ Catalyst via Thermal Activation of Persulfate Ions

Sergio Fernández-Velayos, Nieves Menéndez , Pilar Herrasti and Eva Mazarío * 

Departamento de Química Física Aplicada, Facultad de Ciencias, Universidad Autónoma de Madrid, 28049 Madrid, Spain

* Correspondence: eva.mazarío@uam.es; Tel.: +34-914-975-956

Abstract: In this work, an Fe₃O₄ catalyst was synthesized in a single step via electrochemical synthesis. The Fe₃O₄ catalyst was used to evaluate the degradation of Ofloxacin (OFX) using a heterogeneous advanced oxidation process with sodium persulfate (PS). PS activation was successfully achieved via thermal conventional heating directly and subsequently applied for the degradation of OFX. The degradation kinetics were studied under different conditions, such as catalyst and oxidant concentration and temperature. The results show that a higher reaction temperature, catalyst and initial PS dose strongly influence the degradation efficiency. Thermal activation of persulfate was tested at 20, 40 and 60 °C. At 60 °C, the half-time of OFX was 23 times greater than at 20 °C, confirming the activation of persulfate. Mineralization studies also showed that under optimized conditions (20 mM of persulfate, 1 g/L catalyst and 100 mg/L OFX), a 66% reduction in organic matter was observed, in contrast to that obtained at 40 °C and 20 °C, which was null. The reusability, as tested through the fourth reuse cycle, resulted in a 38% reduced degradation efficiency when comparing the first and last cycle. Furthermore, the electrosynthesized catalyst presented similar degradation efficiencies in both real water and MilliQ, mainly because of the Cl₂⁻ generation at high Cl⁻ concentrations that takes place in Cl⁻ contaminated water.

Keywords: Fe₃O₄; persulfate activation; ofloxacin; mineralization; reusability; real water



Citation: Fernández-Velayos, S.; Menéndez, N.; Herrasti, P.; Mazarío, E. Ofloxacin Degradation over Nanosized Fe₃O₄ Catalyst via Thermal Activation of Persulfate Ions. *Catalysts* **2023**, *13*, 256. <https://doi.org/10.3390/catal13020256>

Academic Editor: Roberto Fiorenza

Received: 30 December 2022

Revised: 17 January 2023

Accepted: 19 January 2023

Published: 22 January 2023



Copyright: © 2023 by the authors. Licensee MDPI, Basel, Switzerland. This article is an open access article distributed under the terms and conditions of the Creative Commons Attribution (CC BY) license (<https://creativecommons.org/licenses/by/4.0/>).

1. Introduction

Antibiotics represent a breakthrough in the treatment for bacterial infection; however, because of their extensive use and high solubility, and their poor biodegradability, antibiotics are nowadays an important concern. Globally, antibiotics are being detected in wastewater, which may produce environmental toxicity, in conjunction with the additional problem of bacteria antibiotic resistance which would seriously hinder the cure of diseases [1]. In 2017, the World Health Organization issued a warning about the re-emergence of flu and tuberculosis, and several studies that observed high resistance levels of those strains encouraged researchers to come up solutions to manage emerging pollutants in effluents [2–4].

The factors primary responsible for the release of high levels of antibiotics and other pharmaceutical wastes into the environment are the pharmaceutical industries [5], municipal wastewater discharges, intensified farming, human excretory wastes, leaching and farmland run-off from fertilized farmland with animal livestock manure and aquaculture nutrition [6].

Antibiotics are difficult to degrade through conventional wastewater treatment. Several techniques have been assayed for the degradation and mineralization of antibiotics to reduce their environmental impact; strategies focused on physical, chemical, biological, and combined processes for degradation have been designed [7–10]. Physical and chemical methods include sedimentation, filtration, and oxidation using chemical compounds, UV or Vis light, ultrasound, and ions. Biological ones include the use of microorganisms or

enzymes [11]. Unfortunately, many of these conventional wastewater treatments are not appropriate for removing highly polar micropollutants, such as antibiotics.

Advanced Oxidation Processes (AOPs) have been proposed for industrial wastewater treatments, such as UV photolysis [12], Fenton [13], Photo-Fenton, [14], or electro-Fenton processes [15]. The Fenton process basically comprises a reaction between iron and hydrogen peroxide to produce hydroxyl radicals (HO^\bullet). Even though in many cases the Fenton method may be effective, its efficiency decreases in certain situations, especially due to the residence times of hydroxyl radicals generated in the solution. In this regard, the use of persulfate (PS), ($S_2O_8^{2-}$), is currently being tested to induce the formation of sulfate radicals, with a longer lifetime and higher redox potential ($E^0 = 2.5\text{--}3.1$ V) compared with hydroxyl radicals (HO^\bullet , $E^0 = 2.8$ V). Sulfate radical formation can be produced via heat [16], ultrasound, ultraviolet, microwave [17], non-contact magnetic heating [18], transition metals, and other techniques [8,19]. Out of all these methods, conventional heat activation is an environmentally friendly and clean-energy method. Additionally, it is an efficient activator, reducing the reaction time and enhancing the degradation efficiency [20]. However, the use of iron ions in solutions results in the formation of sludge that is difficult to extract. To solve this drawback, heterogeneous catalysts such as iron oxides [21], metal iron ferrites [22], perovskites [23,24], metal-carbon nanotubes [25], etc., are often used to activate radical generation superficially, preventing the generation of sludge. The magnetic Fe_3O_4 nanoparticles can be extracted from the medium via magnetic harvesting. In addition, a further advantage is the possibility of working with less acidic medium than that required for the classical Fenton method.

Of the numerous types of commercialized antibiotics, one of the most widely used is Ofloxacin (OFX). OFX is a broad-spectrum fluoroquinolone antibiotic frequently used in clinics for treating bacterial infections. It has already been reported that OFX antibiotics decrease species interaction in the prokaryotic community by reducing the nitrogen fixation, photosynthetic, and metabolic capacities of the microbial community [26]. This antibiotic was chosen as a model for the present work, to study a degradation process with magnetite nanoparticles. The catalyst was synthesized via a facile electrochemical method [27,28]. It exhibited great activity for OFX removal through thermal activation of PS. The correlation between the PS, catalyst concentration, and temperature to the degradation performance was discussed. The reusability of the iron oxide nanoparticles and their performance in real water were also assessed.

2. Results and Discussion

2.1. Fe_3O_4 Catalyst Characterization

The TEM image shown in Figure 1a reveals a sample with certain aggregation and a quasi-spherical shape. The average nanoparticle size measured for at least 150 diameters was 27 nm with an SD of 8 nm, as shown in the inset in Figure 1a. Measurements of the hydrodynamic size (HS) were performed at pH 3.5, the same pH at which the degradation experiments were conducted, which reflects how the particle behaves in a fluid. The mean diameter was 260 (17) nm. The polydispersity index obtained was below 0.2, indicating a relative low polydispersity of the sample in a water matrix. This is in accordance with the Zeta Potential measured at the same pH, whose value was + 28 mV. A high electrostatic repulsion results in a smaller hydrodynamic size and good stability of the suspension. In contrast, the nanoparticle size measured from TEM images was logically smaller than the HS because the particle size was not influenced by the hydration shell in this analysis. The predominant species of OFX at $pH < 5.6$ is the protonated OFX^+ [29]. Consequently, the adsorption between catalyst with a positively charged surface at pH 3.5 and prevalent OFX species under these acidic conditions was not favored due the electrostatic repulsions.

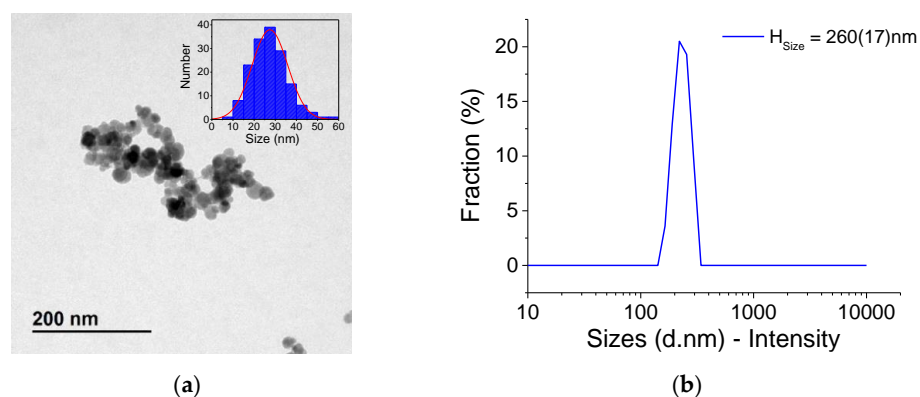


Figure 1. (a) TEM micrography of Fe_3O_4 catalyst, histogram of the average particle size, inset. (b) Hydrodynamic size of Fe_3O_4 measured at pH 3.5.

2.2. Pollutant Removal

It is well known that the solution pH has an important impact on the dissociation of organic pollutants, the surface properties of the catalyst, and the PS activation. In this study, the pH of the solution was maintained at pH 3.5 to ensure catalyst stability via electrostatic forces (zeta potential) in the solution and an efficient PS activation at acidic pH [30,31]. Additionally, the pollutant concentration was kept at 100 mg/L for all the experiments. In contrast, to achieve the best degradation efficiency, several parameters affecting degradation performance, including PS and catalyst concentration, were parameterized individually at 60 °C, to ensure the highest thermal activation of PS.

Thermal activation of PS at 20, 40 and 60 °C was firstly indicated by the single oxidation of PS (20 mM) without catalyst. Figure 2 depicts the evolution of the discoloration of OFX with time. This figure demonstrates the thermal activation of PS as the temperature rose, which progressively decreased the discoloration ratio C/C_0 (ratio of the pollutant concentration at different experimental times to the initial concentration). In contrast, total organic carbon (TOC) removal experiments after 120 min of the reaction revealed a null reduction in the organic carbon content at 20 and 40 °C, whereas the value obtained at 60 °C was about 2%. So even though C/C_0 reduction was observed, as seen in Figure 2, it was unrelated to the mineralization of the organic content. A single thermal activation of PS has been performed by other researchers at different experimental conditions (lower doses of OFX (10 ppm) and higher temperature (70 °C), yielding a TOC removal of 88%) [32]. PS activation can also be fulfilled with a UV-vis source e.g., Liu et al. observed 46.4% TOC removal at room temperature with 5 ppm OFX [33]. From these results, there is evidence that the mineralization of the pollutant may take place without a catalyst, but hereafter, the role of Fe_3O_4 catalysts in the thermal activation of PS will be addressed.

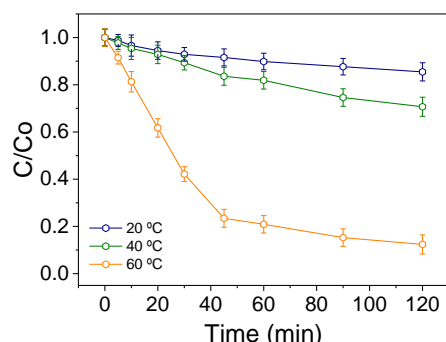


Figure 2. C/C_0 evolution vs. time for OFX concentration with 20 mM of PS at 20, 40, and 60 °C (100 mg/L pollutant) at pH 3.5.

2.3. Effect of Operation Conditions on OFX Degradation

For the study of the effect of operation conditions on OFX degradation, pH and OFX concentration was fixed at 3.5 and 100 mg/L, respectively. In Figure 3a, we can see the obtained kinetic constant for OFX degradation with varied catalyst and PS doses at 60 °C.

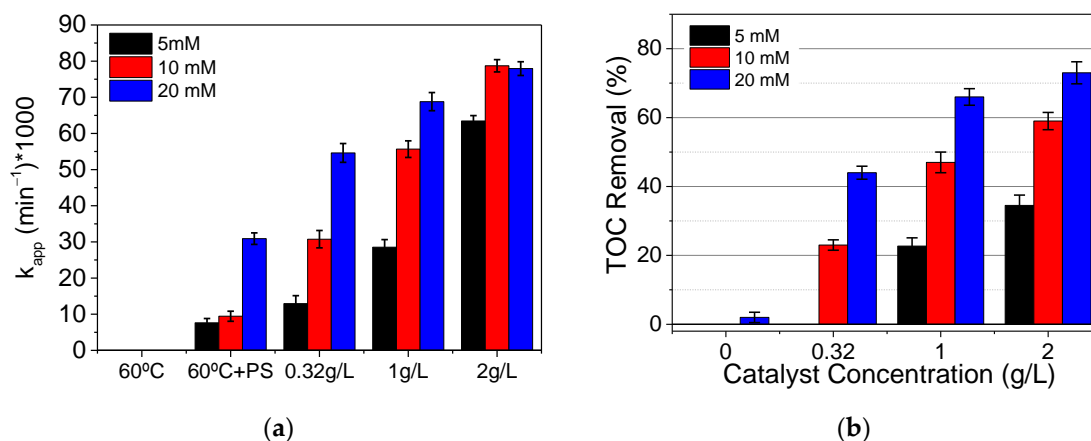


Figure 3. (a) k_{app} constant values obtained from the C/C_0 representation, fitted to a pseudo-first-order model at different catalyst and PS doses; (b) TOC removal efficiency at different catalyst and PS doses (pH 3.5, 100 mg/L OFX and 60 °C).

Assuming that among the reactions taking place during the AOPs, the reaction between sulfate radicals and OFX is the rate-determining step, the rate equation can be given by $v = \frac{dC}{dt} = k[SO_4^{\bullet-}][OFX]$, where C is the concentration of the organic compound and k is the reaction rate constant. We can assume that $SO_4^{\bullet-}$ rapidly achieves a constant steady-state concentration in solution, and the previous equation can be written as a pseudo-first-order reaction rate $\frac{dC}{dt} = k[SO_4^{\bullet-}][OFX] = k_{app}[OFX]$, where k_{app} (min^{-1}) is the apparent pseudo-first-order constant [34,35]. The degradation rate constant was determined from the slope of $\ln\left(\frac{C_t}{C_0}\right) = -k_{app} \cdot t$, where, C_0 (mg/L) is the initial concentration of OFX, C_t (mg/L) is the concentration at time t (min), and k_{app} (min^{-1}) is the apparent constant considering that the [PS] and [catalyst] concentration do not change with the reaction time. All those k_{app} values are also summarized in Table 1, where high r^2 values indicate that the degradation process of OFX could be fitted well to the pseudo-first-order kinetic model. Initially, the effect of temperature (60 °C) was evaluated by itself, showing a null reduction in the C/C_0 ratio, which demonstrates that OFX was difficult to evaporate or decompose at the experimental temperature. It was only when PS was added that a decrease in C/C_0 was observed, allowing the estimation of the kinetic rates. The higher the concentration of PS, the greater the increase in the kinetic rate, as seen in Table 1, being more pronounced when the PS concentration was increased up to 20 mM. A similar effect was observed for the different catalyst doses. At a catalyst concentration of 0.32 g/L, the kinetic rate proportionately increased with the PS concentration, with values of 0.0130, 0.0307 and 0.0546 min^{-1} for 5, 10 and 20 mM, respectively. At a 1 g/L catalyst dose, the increase in PS concentration had a less marked effect on the k_{app} observed for 10 and 20 mM in comparison with the 0.32 g/L dose. Furthermore, at the highest catalyst concentration, this effect was negligible, with k_{app} values of 0.787 and 0.780 min^{-1} being obtained for PS doses of 10 and 20 mM, respectively. Under these experimental conditions, we can consider three important factors: (I) Fe_3O_4 particles probably tend to aggregate at high concentrations, reducing the dosage benefit, (II) the fixed amount of catalyst constrains the rate of radical concentration even at excess PS loading [36], and (III) an increase in catalyst concentration provides more active sites for PS activation, thus increasing the generation of active radicals. As a result of this, an excess of $SO_4^{\bullet-}$ might serve as a scavenger competing in the $SO_4^{\bullet-}/OFX$ interaction, resulting in a null increase in the k_{app} between 10 and

20 mM of PS at 2 g/L. Total organic content removal was also established to evaluate the real organic reduction in the water matrix; those values are reported in Table 1 and Figure 3b for all the experiments conducted.

Table 1. k_{app} and TOC removal (%) values obtained under the studied experimental conditions. (In parentheses are (r^2) values obtained from the pseudo-first-order fitting).

PS dose (mM)	k_{app} (min^{-1})				TOC Removal (%)			
	0 g/L (r^2)	0.32 g/L (r^2)	1 g/L (r^2)	2 g/L (r^2)	0 g/L	0.32 g/L	1 g/L	2 g/L
5 mM	0.0076 (0.977)	0.0130 (0.992)	0.0285 (0.993)	0.0634 (0.990)	0	0	22.7	34.5
10 mM	0.0094 (0.971)	0.0307 (0.983)	0.0557 (0.981)	0.0787 (0.982)	0	23	47	59
20 mM	0.0310 (0.979)	0.0546 (0.984)	0.0688 (0.979)	0.0780 (0.978)	2	44	66	73

First, a reduction was observed from 0.32 g/L and 10 mM and onward, being only 23%. Therefore, it is evident that an increase in the catalyst and PS dose improves the total organic content reduction. However, again, these increases were less pronounced with 1 and 2 g/L catalyst doses when the PS dosage was increased from 10 to 20 mM, with TOC being observed to decrease by 1.40-fold and 1.24-fold at 1 and 2 g/L, respectively. In other words, TOC degradation at 2 g/L in comparison to 1 g/L at 20 mM PS increased by only 7%, which is close to the standard deviation of the analysis. Thus, considering the optimization of both the economic costs of the process and the degradation efficiency, the optimum Fe_3O_4 and PS concentration were fixed at 1 g/L and 20 mM, respectively.

2.4. Effect of the Temperature

With the operation conditions optimized, we compared OFX degradation at three different temperatures: 20, 40 and 60 °C. Figure 4 shows a decrease in the C/C_0 value over time with a rise in temperature. Control experiments are also depicted. TOC removal after 120 min was also different at the different temperatures, being 66% at 60 °C and null at 20 and 40 °C. So, increasing the temperature is conducive to thermal activation of PS and improved pollutant removal. The apparent reaction rate constants, k_{app} at 20 °C, 40 °C and 60 °C were calculated with the pseudo-first-order kinetic equation, and corresponded to 0.0030, 0.0101 and 0.0688, with 3.4-fold and 22.9-fold, increases, respectively. Additionally, to have better knowledge of the thermal degradation improvement, the time necessary to reduce the initial concentration of OFX to 50%, the half-life time ($t_{1/2} = \frac{\ln 2}{k_{app}}$), was calculated and is presented in Table 2. The half-time values obtained at 40 °C and 60 °C were 3.3 and 23 times greater in comparison with $t_{1/2}$ at 20 °C, which is a clear indication of the thermal activation of PS.

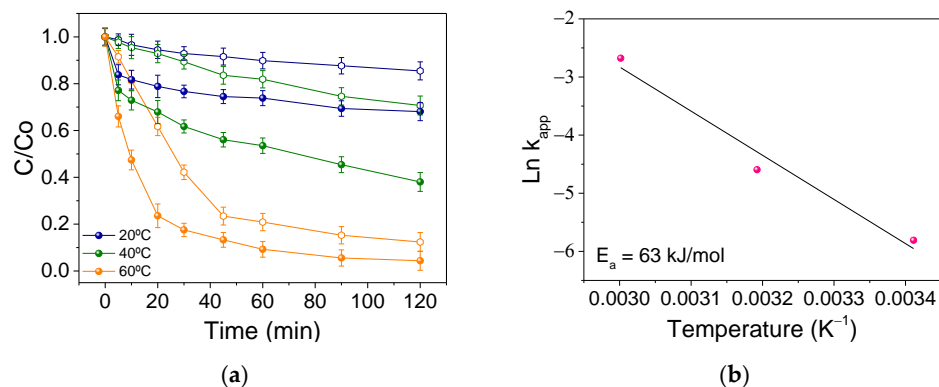


Figure 4. (a) C/C_0 discoloration evolution of OFX at temperatures of 20, 40 and 60 °C (filled dots); control experiments are added for easy comparison (empty dots) (b) Arrhenius plot of OFX degradation. Unless otherwise stated, the reaction conditions are based on: $[\text{OFX}] = 100 \text{ mg/L}$, $[\text{catalyst}] = 1.0 \text{ g/L}$, $[\text{PS}] = 20 \text{ mM}$, time = 2 h, pH = 3.5.

Table 2. k_{app} and half-time values obtained under the studied experimental conditions.

	Without Catalyst–20 mM PS			1 g/L dose–20 mM PS		
T^a (°C)	20	40	60	20	40	60
k_{app} (min ⁻¹)	0.0028	0.0063	0.031	0.0030	0.0101	0.0688
$t_{1/2}$ (min)	247	110	22.3	231	69	10

The apparent activation energy (E_a) was evaluated according to the Arrhenius equation, $\ln k_{app} = \ln A - \frac{E_a}{RT}$, plotting $\ln k_{app}$ against $1/T$, where k_{app} is the apparent rate constant, R is the ideal gas constant (8.314 J/mol.K), A is the pre-exponential factor and T (K) is the temperature. It should be noted that the activation energy (E_a) of the reaction represents the temperature dependence, and a higher value of E_a indicates a higher temperature dependence of the reaction [37]. The E_a value when using Fe_3O_4 as a catalyst was 63 kJ/mol, which is in the normal range of thermal activation energy (60–250 kJ/mol) [38] and is smaller than other values obtained in similar studies [39]. Thus, the OFX degradation by Fe_3O_4 needs moderate activation energy and is easy achieved.

The demonstrated improved oxidation reaction rates at high temperatures, which degraded the organic matter through the generated active free radicals, is a consequence of the endothermicity of the process, which is in accordance with the Arrhenius law, considering the fast generation of active radicals as the temperature rises [19]. The increased diffusion rate and mass transfer rate under high temperatures proved to be beneficial for the removal of pollutants. Through this process, the generation and diffusion of $\text{SO}_4^{\bullet-}$ radicals and electron transport from Fe^{3+} to Fe^{2+} became higher, and most importantly, the molecule collision involving $\text{SO}_4^{\bullet-}$ and pollutant occurred more fiercely. Hence, we may conclude that the positive impact of high temperatures on the removal of pollutants in the advanced oxidation process might result in oxidation promotion.

Table 3 outlines several studies reported in the literature regarding the degradation of OFX when using persulfate. It is worth mentioning, that degradation percentages are exclusively referred to as TOC determinations.

Table 3. Research on the removal of OFX from water using persulfate and different activation methodologies.

Catalyst		PS Conc.	OFX Conc.	Catalyst Conc.	pH	Temperature (°C)	TOC Removal (%)	REF
Fe_3O_4	Thermal/PS	20 mM	100 mg/L	1 g/L	3.5	60	66	This work
—	UV -Vis	0.15 mM	5 mg/L	—	3	25	46.4	[33]
CuFe_2O_4	PS	15 mM	10 mg/L	0.5 g/L	6	25	24.6	[40]
Mn doped CuO	PS	1 mM	10 mg/L	0.5 g/L	8	25	69	[31]
N-doped biochar	PMS	2 mM	40 mg/L	0.4 g/L	5.6	25	63.8	[41]
Nano- FeS_2	Electrochemical	4 mM	10 mg/L	1 g/L	4	25	78.2	[42]
LaMnO_3	PS	0.2 g/L	10 mg/L	0.04 g/L	5	25	41.5	[43]
MnCeOx	PS	1 mM	20 mg/L	0.8 g/L	6.7	25	66	[44]
—	Thermal	4 mM	10 mg/L	—	3	70	88	[32]

Because of the diversity of the studies found in the literature, a comparison can hardly be made. Nevertheless, we must consider that the 66% TOC removal obtained in our research was achieved with an initial concentration of 100 mg/L OFX, whereas in most reported studies, it is possible to achieve a higher degradation % but only with much lower initial OFX concentrations, e.g., 10 mg/L. Furthermore, the simplicity of the synthesis

method for the proposed catalyst, requires less effort than the long and costly synthesis methods referred to in Table 3.

Evidently, the easiest way to compare the benefit of using Fe_3O_4 nanoparticles is by performing a homogeneous test. In a recent paper, we conducted this comparison by estimating the effective surface Fe concentration on the catalyst, based on the weight used as well as factors including particle volume, hydrodynamic size, unit cell stoichiometry, etc. [13]. The outcome shows that only 0.5 ppm Fe was present on the catalyst surface, yielding similar degradation rates in both heterogeneous and homogeneous states at that concentration. In contrast, the facile magnetic recovery and reuse ability make the heterogeneous method a more versatile procedure.

2.5. Reusability

The stability and reusability of a catalyst are critical factors for their applicability in practical environments. Herein, four consecutive degradation runs were conducted to assess the catalytic activity of Fe_3O_4 nanoparticles. The solid catalyst was magnetically separated, thoroughly washed, and dried for subsequent analysis. As shown in Figure 5a, the C/C_0 analysis of the fourth consecutive run was very similar; in addition, the k_{app} obtained for the different runs only slightly decreased, as seen in Table 4. Nevertheless, TOC removal analysis revealed a progressive reduction in the organic matter removed, as seen in Table 4. The decrease in OFX degradation after the first and second cycles was greater than that achieved in the latter cycles, being very similar in the next two cycles, at 44 and 41% TOC removal, respectively. The adsorption of intermediates during degradation, which hinders the active sites, could be a plausible reason for the reduction observed [45]. In any case, the normalized percentage reduction from first to fourth cycle was 38%; this value is not big enough to not consider the electrosynthesized Fe_3O_4 a cost-effective catalyst.

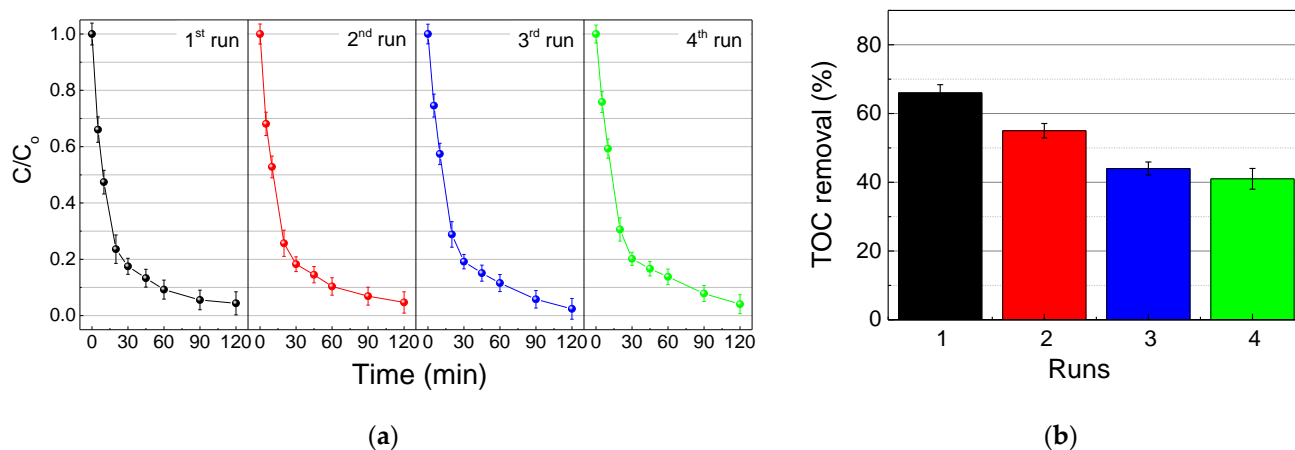


Figure 5. (a) C/C_0 discoloration evolution for OFX degradation with Fe_3O_4 cycling runs. (b) TOC removal efficiency for 2 h of experimentation after four consecutive runs. Unless otherwise stated, the reaction conditions are based on the following: $[\text{OFX}] = 100 \text{ mg/L}$, $[\text{catalyst}] = 1.0 \text{ g/L}$, $T = 60 \text{ }^\circ\text{C}$, $[\text{PS}] = 20 \text{ mM}$, time = 2 h, pH = 3.5.

Table 4. k_{app} and TOC removal (%) values obtained under the studied experimental conditions.

	$k_{app} \text{ (min}^{-1}\text{)}$	TOC Removal (%)
1st	0.0688	66
2nd	0.0660	55
3rd	0.0641	44
4th	0.0614	41

2.6. Catalysis in Real Water

The wastewater itself comprises variable inorganic and organic content, both of which can induce inactivation of the catalyst as well as the suppression of the oxidants, disrupting the catalytic reactions. The representative sample characterization of the matrix is given in Table 5. Then, to demonstrate the catalyst's efficiency in removing OFX, the catalyst was applied to a secondary effluent sample from municipal wastewater treatment plant (WWTP) effluent, and spiked with the pollutant.

Table 5. Representative analysis of the secondary effluent sample tested in this work.

pH	TOC (mg/L)	IC (mg/L)	Conductivity ($\mu\text{S}/\text{cm}$)	Cl^- (mg/L)	Total Solids (mg/L)	Fe (mg/L)
7.6	7.9	19.02	488	270	12	0.049

On the basis of the findings from the operating conditions study, the oxidation tests were carried out with a PS concentration of 20 mM, a catalyst dose of 1 g/L and pH 3.5 at 60 °C. The initial OFX concentration was set at 100 mg/L. The obtained results are shown in Figure 6. It is clear whether the catalytic system was efficient for OFX removal regardless of the water matrix composition. In general, the oxidation is significantly lower in the real water matrix when compared to that in deionized water, but it is not the represented case. Pseudo-first order rate constant values of 0.0688 and 0.0531 min^{-1} were obtained for deionized and real water, respectively. In contrast, there are no differences in TOC removal. Despite, of the important quantity of $\text{HCO}_3^- / \text{CO}_3^{2-}$ (measured as inorganic carbon), in the water matrix, no degradation reduction is observed by scavenging reactions where persulphate radicals are consumed by inorganic matter. Conversely, Cl^- ions was found to have a dual effect (inhibition or enhancement) depending on the Cl^- / PS ratio as described Peng et al. [25]. We can assume this opposite effect considering both, the Cl^- reaction with $\text{SO}_4^{\bullet-}$ and HO^{\bullet} radicals to renders $\text{Cl}_2^{\bullet-}$, a less reactive radical ($E^0 = 1.36 \text{ V}$), together with a greater production of $\text{Cl}_2^{\bullet-}$ at high Cl^- concentrations. On the other hand, the Fe found in real water (0.054 ppm) is not high enough to consider an improved degradation by homogeneous reaction.

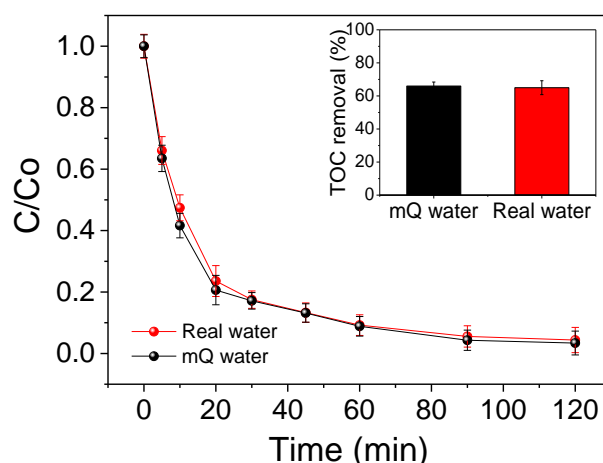


Figure 6. C/Co evolution vs. time for OFX concentration with 20 mM PS at 60 °C (100 mg/L pollutant) at pH 3.5 in mQ and Real water; inset shows TOC removal efficiency for 2 h of experimentation.

3. Materials and Methods

3.1. Synthesis and Characterization of Magnetic Catalyst

Magnetic nanoparticles were synthesized via a previously reported electrochemical method [27,28]. Iron electrodes of 4 and 2 cm^2 were used as the cathode and anode, respectively. A current density of 50 mA/cm^2 was used to promote the oxidation of iron

and the reduction of water to generate hydroxyl ions in solution. The synthesis was carried out in 100 mL of 40 mM NaCl aqueous solution at 25 °C. Solution was stirred at 1100 rpm during 30 min of reaction. The nanoparticles obtained were collected and washed with miliQ water repeatedly until a colorless supernatant was obtained. Then, the nanoparticles were separated from the medium via centrifugation and dried under vacuum overnight. Once dried, the material was characterized using transmission electron microscopy (JEOL JEM 1010 operating at an acceleration voltage of 100 kV) to determine their morphology. Dynamic light-scattering (DLS) measurements were carried out at 25 °C with a Nano ZS (Malvern Panalytical Ltd., Malvern, UK) equipped with a solid-state He-Ne laser ($\lambda = 633$ nm) to determine the hydrodynamic diameter of the water-dispersible nanoparticles. The refraction index was 2.42 and the absorption was 0.8. Nano ZS was also used to measure the zeta potential as a function of the pH at room temperature, using 0.01 M KNO₃ as the electrolyte and HNO₃ and KOH to adjust the pH. Real matrix ionic composition was performed with a TXRF S2 PicoFox spectrometer (Bruker).

3.2. Advanced Oxidation Process Experiments

All degradation experiments were performed using 100 mg/L OFX as the target organic pollutant in the solution. Experiments without a catalyst were performed using 5, 10 and 20 mM PS at 60 °C in order to study a possible single thermal activation. The best degradation conditions were optimized in catalyst presence. PS dose optimization was carried out varying the PS concentration in the range between 5 and 20 mM, while the catalyst concentration was varied in the range 0.32 to 2 g/L. All degradation experiments were performed in 25 mL of solution in a thermostatic bath under continuous stirring at 700 rpm for 2 h. The pH of all solution was adjusted to 3.5 using diluted HNO₃ solutions before the degradation trials began.

3.3. Advanced Oxidation Process Evaluation

Quantitative analysis of OFX degradation was followed by UV-Vis measuring the solution absorbance at $\lambda = 292$ nm for OFX using a Perkin Helmer UV Vis Lambda 365 spectrophotometer. Aliquots of 0.50 mL were withdrawn at 5, 10, 20, 30, 45, 60, 90 and 120 min once the experiment started. These aliquots were diluted to fit on the calibration curve previously obtained ($A = 0.00424 + 0.08755[\text{OFX}]$, $r^2 = 0.9994$), and the absorbances of the diluted samples were measured. Results are presented in this work as the ratio between the concentration obtained for each degradation time and the initial concentration (C/C_0) of 100 mg/L. At the end of the experiment, magnetic nanoparticles were removed using a magnet. The total organic carbon (TOC) of these final solutions was also measured using a TOC-L-CSH model Shimadzu analyzer, considering the average of at least three measurements with an accuracy of $\pm 5\%$. TOC results in this work are shown as TOC removal rate, that is, the ratio between the TOC measured and the initial TOC, 59.8 (1.1) mg/L.

3.4. Reusability Test

The reusability of the catalyst was evaluated by performing four cycling runs. After the completion of the reaction, the separated catalyst was washed with distilled water and dried for the subsequent cycle test. The TOC removal rate was measured after finishing each run.

3.5. Performance in Real Water

The analysis of the catalytic efficiency in a real matrix was performed under catalyst-, PS- and temperature-optimized conditions. The real matrix was previously filtered, with a single filter paper, before use and spiked with 100 mg/L OFX. The solution pH dropped to 3.5 with the addition of diluted nitric acid.

4. Conclusions

In this work, PS was activated using an Fe₃O₄ nanocatalyst at 60 °C and acidic pH for the efficient mineralization of OFX. The results demonstrate that, when the dosage of the catalyst was 1 g/L, the PS concentration was 20 mM and the temperature was 60 °C, nearly 66% of OFX was eliminated at an acidic pH (3.5) over a 120 min reaction. The OFX degradation rate can be effectively tuned by adjusting PS and catalyst loadings. Bicarbonate ions and organic matter present in aqueous media do not suppress the activity of Fe₃O₄ in real water mainly because of the generation of Cl₂^{•−} at high Cl[−] concentrations, which enhances the degradation effect. During the reusability test, the TOC removal rate declined from 66% in the first run to 41% after the fourth run, indicating an efficiency loss of 38% between the two. This value is not big enough to not consider the electrosynthesized Fe₃O₄ nanoparticles as a cost-effective catalyst with a satisfactory reusability potential.

Author Contributions: Conceptualization, S.F.-V., N.M., P.H. and E.M.; methodology, S.F.-V. and E.M.; validation, S.F.-V., P.H. and E.M.; formal analysis, S.F.-V. and E.M.; investigation, S.F.-V. and E.M.; data curation, S.F.-V. and E.M.; writing—original draft preparation, S.F.-V., P.H. and E.M.; writing—review and editing, S.F.-V., N.M., P.H. and E.M.; supervision, S.F.-V. and E.M.; project administration, N.M., P.H. and E.M.; funding acquisition, N.M., P.H. and E.M. All authors have read and agreed to the published version of the manuscript.

Funding: This research was funded by the Madrid Government (Comunidad de Madrid-Spain) under the Multiannual Agreement with Universidad Autónoma de Madrid in the line of action encouraging youth research doctors, in the context of the V PRICIT (Regional Programme of Research and Technological Innovation), (SI1-PJI-2019-00366), and by the Spanish Ministry of Science and Innovation under project no. PID2021-123431OB-I00.

Data Availability Statement: Not applicable.

Conflicts of Interest: The authors declare no conflict of interest.

References

1. Grenni, P.; Ancona, V.; Barra Caracciolo, A. Ecological effects of antibiotics on natural ecosystems: A review. *Microchem. J.* **2018**, *136*, 25–39. [[CrossRef](#)]
2. Wang, P.; He, Y.-L.; Huang, C.-H. Oxidation of fluoroquinolone antibiotics and structurally related amines by chlorine dioxide: Reaction kinetics, product and pathway evaluation. *Water Res.* **2010**, *44*, 5989–5998. [[CrossRef](#)] [[PubMed](#)]
3. Rout, P.R.; Zhang, T.C.; Bhunia, P.; Surampalli, R.Y. Treatment technologies for emerging contaminants in wastewater treatment plants: A review. *Sci. Total Environ.* **2021**, *753*, 141990. [[CrossRef](#)] [[PubMed](#)]
4. WHO. *World Health Statistics 2017: Monitoring Health for the SDGs, Sustainable Development Goals*; World Health Organization: Geneva, Switzerland, 2017.
5. Nikolaou, A.; Meric, S.; Fatta, D. Occurrence patterns of pharmaceuticals in water and wastewater environments. *Anal. Bioanal. Chem.* **2007**, *387*, 1225–1234. [[CrossRef](#)] [[PubMed](#)]
6. Jelić, A.; Petrović, M.; Barceló, D. Pharmaceuticals in Drinking Water. In *Emerging Organic Contaminants and Human Health*; Barceló, D., Ed.; Springer: Berlin/Heidelberg, Germany, 2012; pp. 47–70. ISBN 978-3-642-28132-7.
7. Wu, S.; Hu, Y.H. A comprehensive review on catalysts for electrocatalytic and photoelectrocatalytic degradation of antibiotics. *Chem. Eng. J.* **2021**, *409*, 127739. [[CrossRef](#)]
8. Abdurahman, M.H.; Abdullah, A.Z.; Shoparwe, N.F. A comprehensive review on sonocatalytic, photocatalytic, and sonophoto-catalytic processes for the degradation of antibiotics in water: Synergistic mechanism and degradation pathway. *Chem. Eng. J.* **2021**, *413*, 127412. [[CrossRef](#)]
9. Calcio Gaudino, E.; Canova, E.; Liu, P.; Wu, Z.; Cravotto, G. Degradation of Antibiotics in Wastewater: New Advances in Cavitation Treatments. *Molecules* **2021**, *26*, 617. [[CrossRef](#)]
10. Östman, M.; Björlenius, B.; Fick, J.; Tysklind, M. Effect of full-scale ozonation and pilot-scale granular activated carbon on the removal of biocides, antimycotics and antibiotics in a sewage treatment plant. *Sci. Total Environ.* **2019**, *649*, 1117–1123. [[CrossRef](#)]
11. Homem, V.; Santos, L. Degradation and removal methods of antibiotics from aqueous matrices—A review. *J. Environ. Manage.* **2011**, *92*, 2304–2347. [[CrossRef](#)]
12. Ara, A.; Khattak, R.; Khan, M.S.; Begum, B.; Khan, S.; Han, C. Synthesis, Characterization, and Solar Photo-Activation of Chitosan-Modified Nickel Magnetite Bio-Composite for Degradation of Recalcitrant Organic Pollutants in Water. *Catalysts* **2022**, *12*, 983. [[CrossRef](#)]
13. Rivera, F.L.; Recio, F.J.; Palomares, F.J.; Sánchez-Marcos, J.; Menéndez, N.; Mazarío, E.; Herrasti, P. Fenton-like degradation enhancement of methylene blue dye with magnetic heating induction. *J. Electroanal. Chem.* **2020**, *879*, 114773. [[CrossRef](#)]

14. Bonora, R.; Boaretti, C.; Campea, L.; Roso, M.; Martucci, A.; Modesti, M.; Lorenzetti, A. Combined AOPs for Formaldehyde Degradation Using Heterogeneous Nanostructured Catalysts. *Nanomaterials* **2020**, *10*, 148. [[CrossRef](#)]
15. Rivera, F.L.; Menendez, N.; Mazarío, E.; Herrasti, P. ElectroFenton with Reticular Vitreous Carbon and Iron Oxide Nanoparticles for Dye Removal: A Preliminary Study. *Appl. Sci.* **2022**, *12*, 8293. [[CrossRef](#)]
16. Forouzesh, M.; Ebadi, A.; Abedini, F. Thermocatalytic persulfate activation for metronidazole removal in the continuous operation. *Sep. Purif. Technol.* **2021**, *258*, 118055. [[CrossRef](#)]
17. Qi, C.; Liu, X.; Lin, C.; Zhang, X.; Ma, J.; Tan, H.; Ye, W. Degradation of sulfamethoxazole by microwave-activated persulfate: Kinetics, mechanism and acute toxicity. *Chem. Eng. J.* **2014**, *249*, 6–14. [[CrossRef](#)]
18. Fernández-Velayos, S.; Sánchez-Marcos, J.; Muñoz-Bonilla, A.; Herrasti, P.; Menéndez, N.; Mazarío, E. Direct 3D printing of zero valent iron@polylactic acid catalyst for tetracycline degradation with magnetically inducing active persulfate. *Sci. Total Environ.* **2021**, *806*, 150917. [[CrossRef](#)] [[PubMed](#)]
19. Wang, B.; Wang, Y. A comprehensive review on persulfate activation treatment of wastewater. *Sci. Total Environ.* **2022**, *831*, 154906. [[CrossRef](#)] [[PubMed](#)]
20. Ji, Y.; Ferronato, C.; Salvador, A.; Yang, X.; Chovelon, J.-M. Degradation of ciprofloxacin and sulfamethoxazole by ferrous-activated persulfate: Implications for remediation of groundwater contaminated by antibiotics. *Sci. Total Environ.* **2014**, *472*, 800–808. [[CrossRef](#)]
21. Ouyang, D.; Yan, J.; Qian, L.; Chen, Y.; Han, L.; Su, A.; Zhang, W.; Ni, H.; Chen, M. Degradation of 1,4-dioxane by biochar supported nano magnetite particles activating persulfate. *Chemosphere* **2017**, *184*, 609–617. [[CrossRef](#)]
22. Qin, H.; Yang, Y.; Shi, W.; She, Y. Heterogeneous Fenton degradation of ofloxacin catalyzed by magnetic nanostructured MnFe_2O_4 with different morphologies. *Environ. Sci. Pollut. Res.* **2021**, *28*, 26558–26570. [[CrossRef](#)]
23. Gao, P.; Tian, X.; Nie, Y.; Yang, C.; Zhou, Z.; Wang, Y. Promoted peroxymonosulfate activation into singlet oxygen over perovskite for ofloxacin degradation by controlling the oxygen defect concentration. *Chem. Eng. J.* **2019**, *359*, 828–839. [[CrossRef](#)]
24. Lin, K.-Y.A.; Chen, Y.-C.; Lin, Y.-F. LaMO_3 perovskites (M = Co, Cu, Fe and Ni) as heterogeneous catalysts for activating peroxymonosulfate in water. *Chem. Eng. Sci.* **2017**, *160*, 96–105. [[CrossRef](#)]
25. Peng, J.; Wang, Z.; Wang, S.; Liu, J.; Zhang, Y.; Wang, B.; Gong, Z.; Wang, M.; Dong, H.; Shi, J.; et al. Enhanced removal of methylparaben mediated by cobalt/carbon nanotubes (Co/CNTs) activated peroxymonosulfate in chloride-containing water: Reaction kinetics, mechanisms and pathways. *Chem. Eng. J.* **2021**, *409*, 128176. [[CrossRef](#)]
26. Deng, Y.; Debognies, A.; Zhang, Q.; Zhang, Z.; Zhou, Z.; Zhang, J.; Sun, L.; Lu, T.; Qian, H. Effects of ofloxacin on the structure and function of freshwater microbial communities. *Aquat. Toxicol.* **2022**, *244*, 106084. [[CrossRef](#)]
27. Jaime, J.; Rangel, G.; Muñoz-Bonilla, A.; Mayoral, A.; Herrasti, P. Magnetite as a platform material in the detection of glucose, ethanol and cholesterol. *Sens. Actuators B Chem.* **2017**, *238*, 693–701. [[CrossRef](#)]
28. Rivera, F.L.; Sanchez-Marcos, J.; Menendez, N.; Herrasti, P.; Mazarío, E. Tunneling the size of iron oxide NPs using different alcohols and proportions water-alcohol. *Adv. Nano Res.* **2020**, *8*, 95–102.
29. Chen, P.; Blaney, L.; Cagnetta, G.; Huang, J.; Wang, B.; Wang, Y.; Deng, S.; Yu, G. Degradation of Ofloxacin by Perylene Diimide Supramolecular Nanofiber Sunlight-Driven Photocatalysis. *Environ. Sci. Technol.* **2019**, *53*, 1564–1575. [[CrossRef](#)]
30. Yan, S.; Zhang, X.; Zhang, H. Persulfate activation by Fe(III) with bioelectricity at acidic and near-neutral pH regimes: Homogeneous versus heterogeneous mechanism. *J. Hazard. Mater.* **2019**, *374*, 92–100. [[CrossRef](#)]
31. Liu, B.; Li, Y.; Wu, Y.; Xing, S. Enhanced degradation of ofloxacin by persulfate activation with Mn doped CuO: Synergetic effect between adsorption and non-radical activation. *Chem. Eng. J.* **2021**, *417*, 127972. [[CrossRef](#)]
32. Lin, C.-C.; Ke, J.-Y. Degradation of ofloxacin in water using heat/ $\text{S}_2\text{O}_8^{2-}$ process. *J. Taiwan Inst. Chem. Eng.* **2022**, *140*, 104542. [[CrossRef](#)]
33. Liu, X.; Liu, Y.; Lu, S.; Wang, Z.; Wang, Y.; Zhang, G.; Guo, X.; Guo, W.; Zhang, T.; Xi, B. Degradation difference of ofloxacin and levofloxacin by UV/ H_2O_2 and UV/PS (persulfate): Efficiency, factors and mechanism. *Chem. Eng. J.* **2020**, *385*, 123987. [[CrossRef](#)]
34. Huston, P.L.; Pignatello, J.J. Degradation of selected pesticide active ingredients and commercial formulations in water by the photo-assisted Fenton reaction. *Water Res.* **1999**, *33*, 1238–1246. [[CrossRef](#)]
35. Evgenidou, E.; Konstantinou, I.; Fytianos, K.; Poulios, I. Oxidation of two organophosphorous insecticides by the photo-assisted Fenton reaction. *Water Res.* **2007**, *41*, 2015–2027. [[CrossRef](#)] [[PubMed](#)]
36. Jo, W.-K.; Kumar, S.; Isaacs, M.A.; Lee, A.F.; Karthikeyan, S. Cobalt promoted TiO_2/GO for the photocatalytic degradation of oxytetracycline and Congo Red. *Appl. Catal. B Environ.* **2017**, *201*, 159–168. [[CrossRef](#)]
37. Lee, C.; Yoon, J. Temperature dependence of hydroxyl radical formation in the $h\nu/\text{Fe}_3^+/\text{H}_2\text{O}_2$ and $\text{Fe}_3^+/\text{H}_2\text{O}_2$ systems. *Chemosphere* **2004**, *56*, 923–934. [[CrossRef](#)] [[PubMed](#)]
38. Xu, X.-R.; Li, X.-Z. Degradation of azo dye Orange G in aqueous solutions by persulfate with ferrous ion. *Sep. Purif. Technol.* **2010**, *72*, 105–111. [[CrossRef](#)]
39. Li, T.; Lu, S.; Lin, W.; Ren, H.; Zhou, R. Heat-activated persulfate oxidative degradation of ofloxacin: Kinetics, mechanisms, and toxicity assessment. *Chem. Eng. J.* **2022**, *433*, 133801. [[CrossRef](#)]
40. Wang, Q.; Wang, B.; Ma, Y.; Xing, S. Enhanced superoxide radical production for ofloxacin removal via persulfate activation with Cu-Fe oxide. *Chem. Eng. J.* **2018**, *354*, 473–480. [[CrossRef](#)]
41. Huang, Y.; Li, G.; Li, M.; Yin, J.; Meng, N.; Zhang, D.; Cao, X.; Zhu, F.; Chen, M.; Li, L.; et al. Kelp-derived N-doped biochar activated peroxymonosulfate for ofloxacin degradation. *Sci. Total Environ.* **2021**, *754*, 141999. [[CrossRef](#)]

42. Aseman-Bashiz, E.; Sayyaf, H. Synthesis of nano-FeS₂ and its application as an effective activator of ozone and peroxydisulfate in the electrochemical process for ofloxacin degradation: A comparative study. *Chemosphere* **2021**, *274*, 129772. [[CrossRef](#)]
43. Nie, Y.; Zhou, H.; Tian, S.; Tian, X.; Yang, C.; Li, Y.; Tian, Y.; Wang, Y. Anionic ligands driven efficient ofloxacin degradation over LaMnO₃ suspended particles in water due to the enhanced peroxymonosulfate activation. *Chem. Eng. J.* **2022**, *427*, 130998. [[CrossRef](#)]
44. Niu, L.; Xian, G.; Long, Z.; Zhang, G.; Zhu, J.; Li, J. MnCeOX with high efficiency and stability for activating persulfate to degrade AO₇ and ofloxacin. *Ecotoxicol. Environ. Saf.* **2020**, *191*, 110228. [[CrossRef](#)] [[PubMed](#)]
45. Zazo, J.A.; Casas, J.A.; Mohedano, A.F.; Rodríguez, J.J. Catalytic wet peroxide oxidation of phenol with a Fe/active carbon catalyst. *Appl. Catal. B Environ.* **2006**, *65*, 261–268. [[CrossRef](#)]

Disclaimer/Publisher's Note: The statements, opinions and data contained in all publications are solely those of the individual author(s) and contributor(s) and not of MDPI and/or the editor(s). MDPI and/or the editor(s) disclaim responsibility for any injury to people or property resulting from any ideas, methods, instructions or products referred to in the content.